Reconfigurable Dual Band Bidirectional Reflection Amplifier with Applications in Van Atta Array

Farhad Farzami, *Student Member, IEEE,* Seiran Khaledian, *Student Member, IEEE,* Besma Smida, *Senior Member, IEEE,* Danilo Erricolo, *Fellow, IEEE*

***Abstract*—We designed a reconfigurable dual band reflection amplifier with operation frequency bands over 1.8 GHz and/or 2.4 GHz. This one-port amplifier boosts the reflected signal over either of these two frequency bands or both as a dual band reflection amplifier. The amplifier circuit consists of a FET transistor and two PIN diodes which act as switches to form a reconfigurable system. The measured reflection gains at single 1.8 GHz and 2.4 GHz frequency bands are 17.6 dB and 16.75 dB respectively. The dual band operation frequency shows 11.2 dB and 15 dB gain at 1.8 GHz and 2.4 GHz, respectively. Then, we realized a bidirectional amplifier using a dual band -3 dB 90° Branch Line Coupler (BLC) integrated with two of the proposed reconfigurable reflection amplifiers. This bidirectional amplifier is a two-port bilateral amplifier. The measured reflection gains show at least 10 dB transmission gains (S_{21} and S_{12}) at operation frequency bands. The proposed reconfigurable bidirectional amplifier is then used in a dual band Van Atta array. The proposed active retrodirective system outperformed passive Van Atta array by 5 dB gain with only half the number of antenna elements. Each component is investigated analytically and analyzed by Advanced Design System (ADS). Fabricated circuits are measured and show a good agreement with simulations.**

***Index Terms*—Active Van Atta array, back-scatter communication, bilateral amplifier, dual band communication, dual band hybrid, CRLH TL, Ga-As FET, negative input impedance, PIN diode, reconfigurable bidirectional amplifier, reflection amplifier, retrodirective array.**

I. Introduction

BACK-SCATTER Communications (BSC) are based on the reflection of electromagnetic waves. In a point-to-point BSC, the carrier power is generated at the receiving end, and the transmitter is replaced by a modulated reflector [1]. This setup is capable of modulating data upon the original waveform, which can be received and decoded. This leads to low-profile and low-power communication terminals.

The most prominent application of this technology is Radio Frequency Identification (RFID) [2]. BSC is also implemented in a number of other areas, such as wireless sensor networks [3], target detection [4], satellite [5] and full-duplex communications [6].

The widespread use of BSC systems introduce more interference among densely deployed BSC terminals. They also suffer from the interference generated by other popular wireless systems such as WLAN and NFC [7]. In addition, BSC has been restricted to short-range communications because of the *combined* path-loss associated with the forward and backward links.

To improve BSC range, many works have been proposed in the literature to increase the value of the Radar Cross-Section (RCS). Two popular approaches employ active scatterers [8]–[11] or/and RetroDirective Antenna (RDA) arrays [12], [13].

The first approach – based on active scatterers – uses a reflection amplifier to amplify the backscattered signal. A reflection amplifier is a one-port active device. Its negative input resistance makes the input reflection coefficient larger than unity ($|\Gamma_{in}| > 1$) [14]–[16]. This negative input resistance can be implemented by transistors [8], [14], Gunn diodes [17] or tunnel diodes [15]. These reflection amplifiers are designed to operate in one single frequency band. In this work, we used GaAs Heterojunction FET (HJ-FET) transistor to implement the negative input resistance.

The second approach – based on RDA arrays – increases the RCS by using self-steering capabilities, which means that the antenna array reflects the received signal back towards the source direction without any prior knowledge about the source location. Many RDA array systems are based on the Van Atta array [18].

Since BSC systems with Van Atta arrays still suffer from short range communication, active Van Atta arrays by means of unilateral amplifiers have been proposed, for example in [9], [19]–[21].

An active Van Atta array by means of a bidirectional amplifier is proposed in [13], [22]. The bidirectional amplifier is a bilateral amplifier that has gain in both directions to use all array elements. It is composed of a 90°, -3 dB Branch Line Coupler (BLC) and two identical reflection amplifiers. So far, all proposed reflection amplifiers and active Van Atta arrays have been designed for a *single* frequency band.

In this paper, we propose a novel reconfigurable dual band active Van Atta array that increases the range and reduces the interference in BSC systems. Our contribution is threefold: we first propose a novel *reconfigurable dual band* reflection amplifier (1.8 GHz and/or 2.4 GHz). The proposed reflection amplifier provides four modes of operations: i) reflection gain in both frequency bands; ii) and iii) reflection gain in one frequency band or the other; and, iv) no reflection gain. Then, based on the proposed dual band reflection amplifier, we design a reconfigurable dual band bidirectional amplifier by combining two of the proposed reflection amplifier and a dual band BLC. Finally, we design a reconfigurable dual band active Van Atta array by using the proposed bidirectional

F. Farzami, S. Khaledian, B. Smida and D. Erricolo are with Department of Electrical and Computer Engineering, University of Illinois at Chicago, Chicago, IL 60607 USA (e-mail: ffarza2@uic.edu, skhale6@uic.edu, smida@uic.edu and derric1@uic.edu).

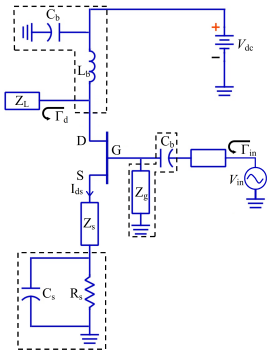

Fig. 1: The schematic of the reflection amplifier.

amplifier and dual band antenna elements. Each component is investigated and analyzed by Advanced Design System (ADS). Fabricated circuits are measured and show a good agreement with simulations.

The proposed reconfigurable dual band bidirectional amplifier provides at least 10 dB gain by using 2.4 mW power consumption. The proposed active Van Atta array shows 5 dB higher back-scattered field level on average for the both frequency bands, compared to a passive one with the double number of elements. Furthermore, it offers the possibility to change the frequency band in crowded frequency spectrum environments. In addition, it allows the use of two frequency bands simultaneously to increase the throughput and/or the range [23], [24].

This article is organized as in the following: In section II, we investigate the reconfigurable dual band reflection amplifier, implement it, build it and test it. The reconfigurable dual band bidirectional amplifier and active Van Atta array are investigated in section III. Conclusions are provided in section IV.

II. Reflection Amplifier

A. Single Band Reflection Amplifier

The performance of reflection amplifiers is characterized by the reflection gain defined as

$$|\Gamma_{in}|^2 = \left|\frac{Z_{in} - Z_0}{Z_{in} + Z_0}\right|^2, \quad (1)$$

where Z_0 is the impedance of the load connected to the reflection amplifier and Z_{in} is the input impedance of the reflection amplifier. The reflection gain must exceed unity in a reflection amplifier and this occurs when the input resistance satisfies $Re(Z_{in}) < 0$. In fact, if $Z_{in} \to -Z_0$ then $|\Gamma_{in}|^2 \to \infty$. However, to avoid oscillations and degrading the signal to noise ratio (SNR), the value of Z_{in} must be kept different from $-Z_0$ by some margin [11], [25], [26]. Reflection amplifiers may be implemented using transistors such as in Fig. 1, which is based on a configuration already discussed in [9], [13], [27] consisting of a common source FET loaded at its drain by an open circuit microstrip line. The transistor is intentionally kept in the potentially unstable region by using a feedback load Z_s so that the transistor has $|\Gamma_{in}| > 1$ for some values of the load impedance Z_L [28], as shown in Fig. 1.

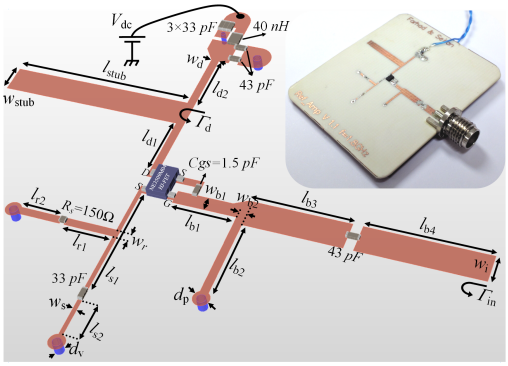

(a)

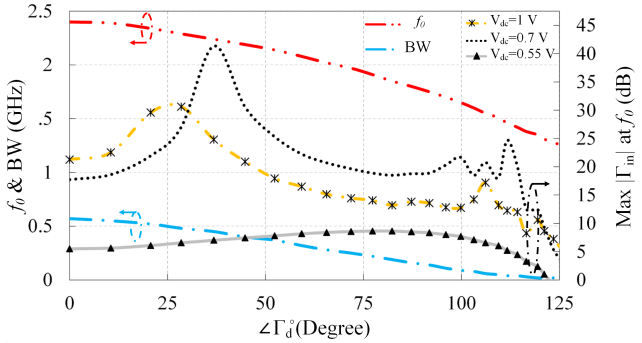

(b)

Fig. 2: (a) The layout of the reflection amplifier, (b) the maximum of $|\Gamma_{in}|$ in term of frequency and magnitude vs. $\angle\Gamma_d$ and the bandwidth of $|\Gamma_{in}| > 0$ dB for different V_{dc}. The dimensions in mm are: $l_{b1} = 4,\ l_{b2} = 5.5,\ l_{b3} = 6,\ l_{b4} = 7.5,\ l_{s1} = 7.5,\ l_{s2} = l_{r1} = l_{r2} = 3,\ l_{d1} = l_{d2} = 4,\ w_s = 0.25,\ w_r = w_d = w_{b2} = 0.5,\ w_{b1} = 0.9$ and $w_i = w_{stub} = 1.8$.

In this work, we focused on two frequently used frequency bands, 1.8 GHz and 2.4 GHz. We have implemented the circuit of Fig. 1 on a Rogers 4003C substrate with $\epsilon_r = 3.55$ and thickness of $h = 0.812$ mm (32 mil) and used the GaAs HJ-FET with part number NE3509M04 from Renesas resulting into the layout of Fig. 2(a), where an external capacitor C_{gs} is added between the gate and the source so that it is possible to have reflection gain at lower frequencies. The capacitors and inductors were from Murata (GRM03 series) and Coilcraft (0402HP series), respectively. The circuit is designed so that $|\Gamma_{in}|$ is a function of the reflection coefficient phase of the terminated load $|\Gamma_{in}| = \Gamma_{in}(\angle\Gamma_d)$, since $|\Gamma_d| \simeq 1$ for an open-ended microstrip line and it is shown in Fig. 2(b), where the maximum of $|\Gamma_{in}|$ occurs at f_0. The same figure indicates the bandwidth BW as $|\Gamma_{in}| > 0$ dB. The transistor behavior depends on the bias point so that $|\Gamma_{in}|_{max}$ varies as a function of V_{dc} as shown in the same figure for three values of V_{dc}. The bias voltage has effect also on 1 dB compression point P1dB and the stability criteria.

In order to obtain the desired behavior of $|\Gamma_{in}|$, the lengths of the terminated load at the drain l_{d1} and l_{d2} are chosen to have the maximum reflection gain at $f_0 = 1.8$ GHz when $l_{stub} = 12$ mm ($\angle\Gamma_d \simeq \pi/2$) and $f_0 = 2.4$ GHz ($\angle\Gamma_d = 0$) when $l_{stub} = 0$ mm as shown in Fig. 2(b).

We fabricated two reflection amplifiers and a comparison between simulation and measurement results is shown in Fig.

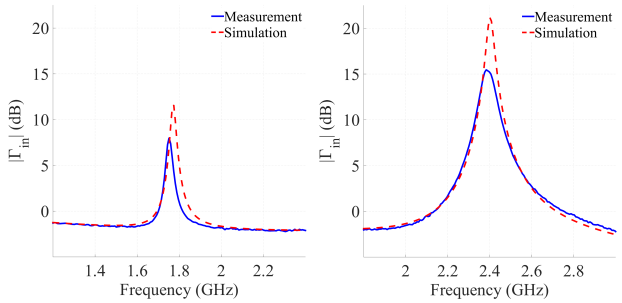

Fig. 3: $|\Gamma_{in}|$ for the reflection amplifier with $V_{dc} = 1$ V and $I_{ds} = 2$ mA at (a) 1.8 GHz frequency band when $l_{stub} = 12$ mm, and (b) 2.4 GHz frequency band when $l_{stub} = 0$ mm.

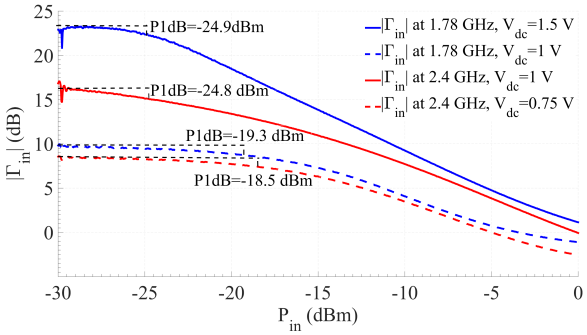

Fig. 4: The measured reflected gain vs. the incident power of the reflection amplifiers.

3. The reflection amplifier can be designed for any other desired frequency band following the same procedure.

We measured the spectral content of the output of the reflection amplifier to verify that it does not oscillate by connecting it to an Agilent Technologies E4440A PSA spectrum analyzer, which has an input impedance of $Z_0 = 50\ \Omega$. We observed that oscillations start when $V_{dc} > 1.65\ V$ and $V_{dc} > 1.2\ V$ for the 1.8 GHz and 2.4 GHz frequency band, respectively. Therefore, by keeping the bias voltage below these values, the frequency spectrum is clear from DC to 26.5 GHz. However, for active RFID applications or other active back-scatterer, the input impedance of the load (antenna) may be different from 50 Ω and the appropriate bias voltages must be determined [11].

We determined the 1 dB compression point by measuring the reflected gain based upon the incident power, as shown in Fig. 4. The results have been investigated for several biasing points for both frequency bands using an Agilent Technologies vector network analyzer PNA 5222A with the minimum source power of -30 dBm.

Simulations were performed with ADS EMcosim technique to maximize the results accuracy. The DC power consumption for both circuits with $V_{dc} = 1$ V is 2.4 mW.

B. Dual Band Reflection Amplifier

Since $|\Gamma_{in}|$ is a function of $\angle\Gamma_d$, by setting a terminated load that provides simultaneously the desired phase values

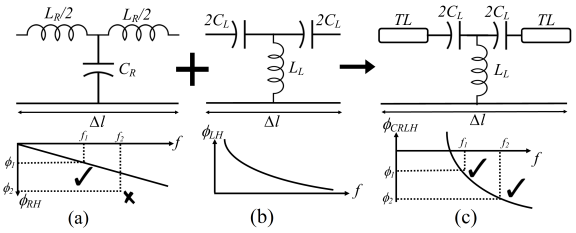

Fig. 5: Phase response of (a) RH TL, (b) LH TL and (c) CRLH TL.

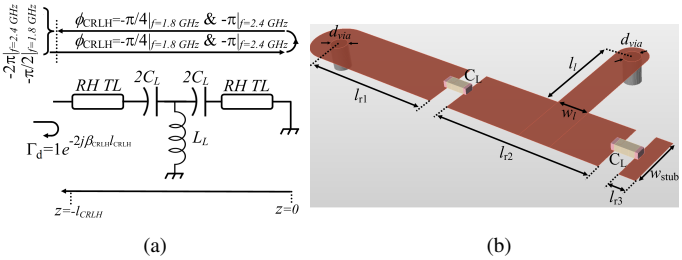

Fig. 6: (a) The short-ended CRLH TL schematic, (b) the layout of this line. the dimensions in mm are: $l_{r1} = 4.5$, $l_{r2} = 5$, $l_{r3} = 0.5$, $l_l = 3$, $w_l = 1$, $d_{via} = 0.55$ and $w_{stub} = 1.8$.

$\angle\Gamma_d|_{f_1} = \phi_1$ and $\angle\Gamma_d|_{f_2} = \phi_2$ to have reflection gain at f_1 and f_2, we obtain a dual band reflection amplifier.

A Composite Right Left Hand (CRLH) Transmission Line (TL) is used to reach the two desired values of the phase at two arbitrary different frequencies. A CRLH TL consists of a conventional Right Hand (RH) TL and an embedded Left Hand (LH) TL as lumped or distributed elements. The combination of RH and LH TLs provides a non-linear phase response with two degrees of freedom [29]. In fact, with an RH TL it is only possible to control the slope of its phase response ϕ_{RH}, which prevents setting the two arbitrary values of the phases $\phi_1|_{f_1}$ and $\phi_2|_{f_2}$, see Fig. 5(a).

The LH TL shows a non linear positive phase response ϕ_{LH}, Fig. 5(b). As a result, CRLH TL provides a non-linear phase response $\phi_{CRLH} = \phi_{RH} + \phi_{LH}$ with two degrees of freedom, Fig. 5(c).

If the progressive phases of the RH and LH unit cells are much smaller than $\pi/2$, the phase of a composite line can be approximated as [30]

$$\phi_{CRLH} = \phi_{LH} + \phi_{RH} = -Pf + \frac{Q}{f}, \tag{2}$$

$$P = 2\pi N\sqrt{L_R C_R},\ Q = \frac{N}{2\pi\sqrt{L_L C_L}}, \tag{3}$$

where N is the number of unit cells. C_R, L_R, C_L and L_L are the values of the capacitors and inductors of the RH and LH TL, respectively.

We used a short-ended CRLH TL as the terminated load Z_L of the reflection amplifier, Fig. 6. From the results of the previous section, in order to achieve a dual band reflection amplifier at 1.8 GHz and 2.4 GHz, $\angle\Gamma_d|_{f_0=1.8\ \text{GHz}} \simeq -\pi/2$ and $\angle\Gamma_d|_{f_0=2.4\ \text{GHz}} \simeq -2\pi$. Since the phase of the reflection coefficient of a terminated line is twice of the progressive phase in one direction, the short-ended CRLH TL phase should

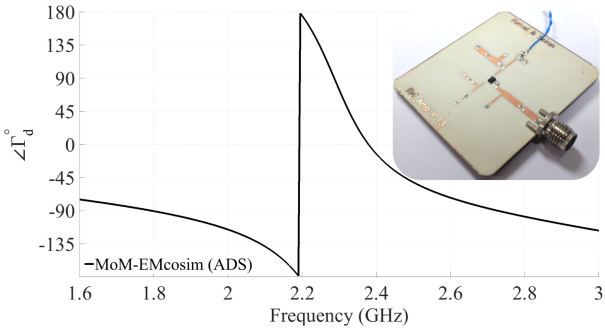

Fig. 7: The phase response of the short-ended CRLH TL. $\angle\Gamma_d|_{f=1.8\text{ GHz}} \simeq -90^\circ$ and $\angle\Gamma_d|_{f=2.4\text{ GHz}} \simeq -10^\circ$.

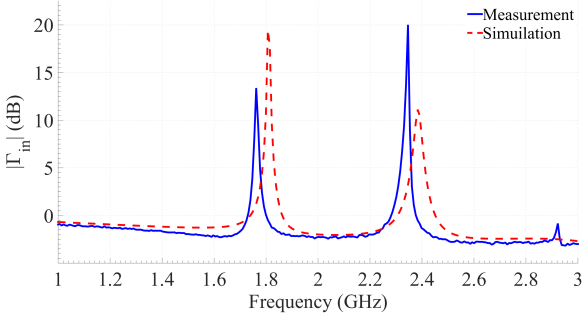

Fig. 8: The measurement and simulation of $|\Gamma_{in}|$ for the dual band reflection amplifier, $V_{dc} = 3$ V and $I_{ds} = 2.4$ mA

.

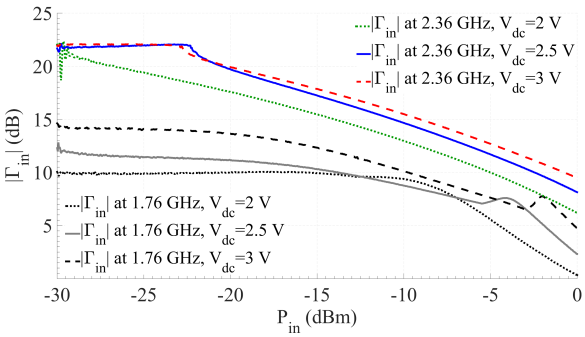

Fig. 9: The reflected gain based on the incident power of the dual band reflection amplifier. The P1dB for the 1.8 GHz (2.4 GHz) frequency band are -8.6 (-26.7), -16 (-21.5) and -17.8 (-22.2) dBm for $V_{dc} =$ 2, 2.5 and 3 V, respectively.

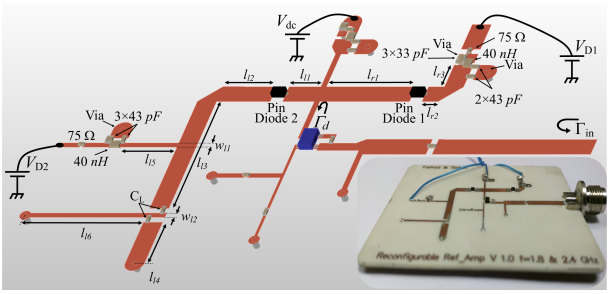

Fig. 10: The layout of the reconfigurable dual band reflection amplifier. The dimensions in mm are: $l_{r1} = 8.5$, $l_{r2} = 1.5$, $l_{r3} = 2.65$, $l_{l1} = 3$, $l_{l2} = 5$, $l_{l3} = 13$, $l_{l4} = 5$, $l_{l5} = 5$, $l_{l6} = 11$ and $w_{l1} = w_{l2} = 0.5$. Other dimensions are as same as the Fig. 2(a).

show $-\pi/4$ and $-\pi$ at 1.8 GHz and 2.4 GHz, respectively, Fig. 6(a).

The layout of the short circuit CRLH TL is shown in Fig. 6(b). We considered $N = 1$ and the LH TL is realized by using two series capacitors C_L and a shunt inductor L_L. The inductor is realized by using a short-ended microstrip line with length l_l.

Using Eq. (2), we obtain $P = 2.43 \times 10^{-9}$ s and $Q = 6.46 \times 10^9$ Hz. The characteristic impedance of the LH TL (Z_{LH}) is set to 50 Ω, so that L_L and C_L can be derived from [29]

$$L_L = Z_{LH}\sqrt{L_L C_L} = 1.23\ nH, C_L = \frac{\sqrt{L_L C_L}}{Z_{LH}} = 0.5\ pF. \tag{4}$$

Two GRM03 series capacitors from Murata with value of 1 ± 0.05 pF are used as the capacitors of the LH TL. The value of L_L is achieved by the short-ended microstrip line with length $l_l = 3$ mm and width $w_l = 1$ mm. The associated phase of the RH TL is equal to $\phi_{RH} = -Pf_{1or2}$. At 1.8 GHz, $\phi_{RH} \approx -110^\circ$ which leads to a 10 mm short-ended microstrip line with the width of 1.8 mm for having $Z_0 = 50$ Ω.

The $\angle\Gamma^{SC}_{CRLH\ TL}$ is shown in Fig. 7. Simulation and measurement results are shown in Fig. 8. The differences between the simulation and measurement is less than 40 MHz which is only 2.2 % and 1.6 % of the frequency shift from $f_0 = 1.8$ GHz and $f_0 = 2.4$ GHz, respectively.

The reflected gain vs. incident power for each frequency bands and three different bias voltages are shown in Fig. 9. The measurements show that the dual band reflection amplifier starts oscillating when V_{dc} exceeds 3.25 V while it is connected to the spectrum analyzer.

C. Reconfigurable Dual Band Reflection Amplifier

We introduced two single-band and one dual band reflection amplifiers in the previous section. All of them can modulate the back scattered signal by On and Off Keying (OOK) [9], [31]. However, in the dual band reflection amplifier, both bands must be either on or off at the same time. Thus, the active scatterer will not be able to modulate the back-scattered signal in two frequency bands independently.

In this section, we introduce, to the best of the knowledge of the authors, a novel reconfigurable dual band reflection amplifier where the two frequency bands are independently operated. Since there are two independent bands and each one of them is modulated with OOK then there are four possible states of operation for the amplifier.

The layout of the proposed reconfigurable reflection amplifier is shown in Fig. 10. This layout contains two PIN diodes, which are used as switches to open or close lines to achieve adjustable phase-response $\angle\Gamma_d$ in the terminated load. The PIN diodes are controlled by their bias voltages, which could be either high (5 V) when the diode is off, or low (0 V), when the diode in on. Hence, there are four possible states for the

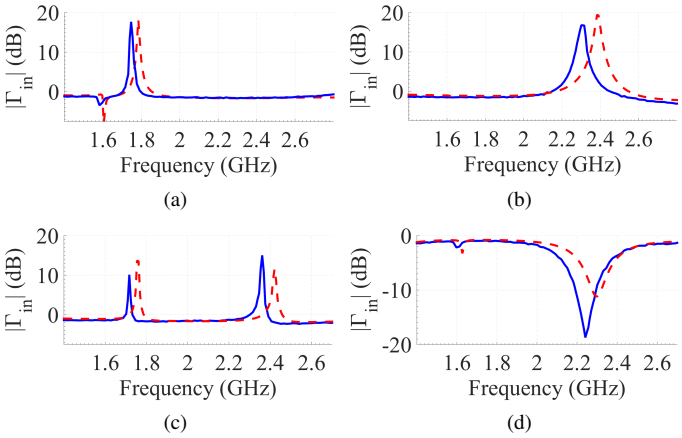

Fig. 11: The reflection gain of the reconfigurable dual band reflection amplifier when $V_{dc} = 3$ V. (a) $V_{D1} = V_{D2} = 5$ V, (b) $V_{D1} = 0$ V, $V_{D2} = 5$ V, (c) $V_{D1} = 5$ V, $V_{D2} = 0$ V and (d) the reflection amplifier is off ($V_{dc} = 0$ V).

PIN diodes. In order to obtain the four states for the OOK modulation, one state is provided when the whole amplifier is off and the other three states are provided by the on and off combinations of the PIN diodes, excluding the one where both diodes are on.

Referring to Fig. 10, the single band mode of operation requires only the use of the right arm, with the left arm maintained inoperative, hence PIN diode 2 must be off. PIN diode 1 changes the length of the right arm, which is a RH TL, so that the reflection amplifier frequency band of operation is 1.8 GHz when PIN diode 1 is off, see Fig. 11(a), and 2.4 GHz when PIN diode 1 is on, see Fig. 11(b). The dual band mode of operation requires only the use of the left arm and thus PIN diode 1 is off and PIN diode 2 is on, see Fig. 11(c). The left arm consists of two series capacitors and a distributed shunt inductor to realize the CRLH TL. The fourth state with the reflection amplifier turned off has the reflection gain shown in Fig. 11(d).

The proposed reconfigurable reflection amplifier was fabricated and measured. The measurements show that the amplifier starts to oscillate in single band mode of operation when $V_{dc} > 3.25$ V at each of the frequency bands, when the amplifier is connected to the spectrum analyzer. For dual band mode of operation, oscillations start if $V_{dc} > 3.75$ V. Thus, with $V_{dc} = 3$ V, the reflection amplifier is stable for all three active states.

III. Reconfigurable Dual Band Active Van Atta Array

A. Reconfigurable Dual Band Bidirectional Amplifier

We obtain next a novel reconfigurable dual band bidirectional amplifier using the proposed reconfigurable dual band reflection amplifier with a dual band BLC.

Bidirectional (bilateral) amplifiers have many applications including active back-scatterer systems, full duplex and half duplex communication systems [13], [32], [33]. They are two-port networks that amplify signals in both directions, resulting

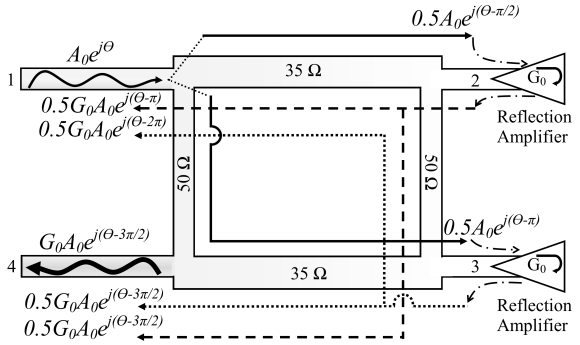

Fig. 12: The configuration of a bidirectional amplifier by using a BLC and two identical reflection amplifiers.

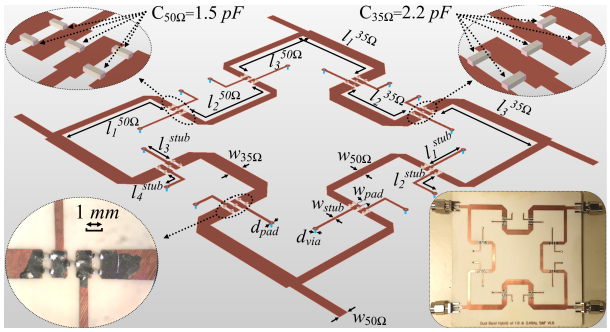

Fig. 13: The layout of the dual band hybrid. The dimensions in mm are: $l_{1,2}^{50\Omega} = 26.6$, $l_3^{50\Omega} = 27.75$, $l_{1,2}^{35\Omega} = 25$, $l_3^{35\Omega} = 22.5$, $l_{stub1,2} = 8.75$ $l_{stub3,4} = 6$, $w_{stub} = 0.55$, $d_{via} = 0.3$, $d_{pad} = 1$, $w_{50\Omega} = 1.8$ and $w_{35\Omega} = 3.1$.

into $S_{12} = S_{21}$, which is contrary to the behavior of a unilateral amplifier.

A bidirectional amplifier may be obtained using two identical reflection amplifiers integrated with a BLC [13], [34] as shown in Fig. 12. Assuming an ideal BLC and perfectly identical reflection amplifiers, two reflection amplifiers with power gain G_0 are connected to the second and third port of the BLC; the input signal at port 1 is divided into two signals with equal power ($0.5A_0$), but with a $\pi/2$ phase shift at the second and third ports. The reflected signals cancel out each other at port 1 due to the π phase shift, while they add up at port 4 because there is no relative phase shift. The input signal at port 4 appears with the same gain at port 1 due to the symmetry of the BLC. However, actual BLCs present non-ideal behaviors such as reflections at their ports, limited isolation between ports 1 and 4, different gain values for the reflection amplifiers, which all contribute to increase the VSWR at the input and output ports of a bidirectional amplifier, as shown in [13].

We integrated the proposed reconfigurable dual band reflection amplifier with a dual band BLC realized by CRLH TL, to achieve a novel reconfigurable dual band bidirectional amplifier. The dual band BLC is discussed in [29]. The frequency bands are the same as in the reconfigurable reflection amplifier. The values of the CRLH TL components should be selected to provide a quarter wavelength at these frequencies. For example, by substituting $\phi_1 = \phi_2 = -\pi/2$ into Eq. (2),

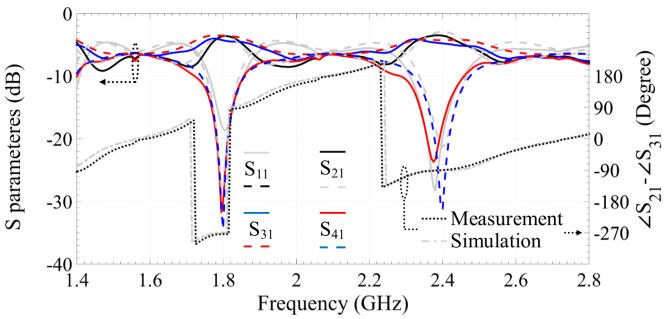

Fig. 14: The S parameters of the dual band BLC. The solid (dashed) lines are measurements (simulations).

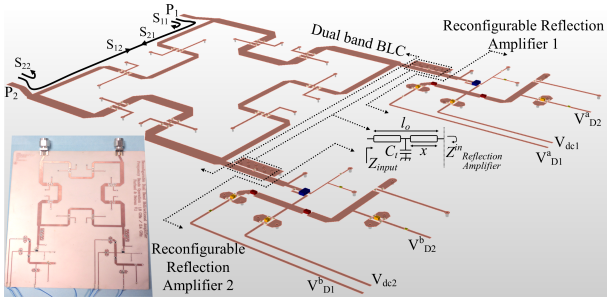

Fig. 15: The layout of the bidirectional amplifier. The tuning capacitors are $C_t = 1$ pF. The transition line length (l_0) is 13 mm. The position of capacitor (x) for amplifier 1 is 6 mm and 4 mm for amplifier 2.

$P \simeq 3.36 \times 10^{-9}$ s and $Q \simeq 8.08 \times 10^{9}$ Hz.

The lumped element approximation is valid when ϕ_{LH}(unit cell) $\ll \pi/2$. By using the LH part of Eq. (2) and Eq. (3), $N > L/2f_1$ or $N > 2.24$ in this case. We selected $N = 4$, which means each CRLH TL consists of four lumped elements LH unit cell. Since the characteristic impedance of BLC lines are 50 Ω and 35 Ω, there are two sets of values for the series capacitors and shunt inductor. For the the 50 Ω-line, $C_L = 1.5$ pF and $L_L = 3.95$ nH while for the 35 Ω-line, $C_L = 2.2$ pF and $L_L = 2.75$ nH. The value of $\phi_{RH} = 347°$ at $f = 1.8$ GHz, so for the 50 Ω (35 Ω)-RH TL the width and length are 1.8 mm (3.2 mm) and 96 mm (94 mm), respectively. The layout of the dual band BLC is shown in Fig. 13. The meander TL helps to shrink the circuit length from 96 mm to 65 mm. The capacitors are from the Murata GRM03 series ±0.1 pF tolerance. The shunt inductors are realized by the short-ended microstrip lines and some of them are bent to avoid crossing each other. The CRLH TL has a natural LH cutoff frequency given by [30]:

$$f_c^{LH} = \frac{1}{4\pi\sqrt{L_L C_L}} = 1 \text{ GHz}, \tag{5}$$

which is lower than $f_1 = 1.8$ GHz. On the other hand, the self-resonant frequency of the capacitor chips, approximately 8 GHz, is the higher frequency limit, which is above $f_2 = 2.4$ GHz.

The measurement and simulation results of the dual band BLC are shown in Fig. 14. The phase difference between the two output ports 2 and 3 is $\pm\pi/2$, which is required to have cancellation at the in/output ports 1 and 4 in the bidirectional amplifier. The dual band BLC and the reconfigurable dual band reflection amplifiers are integrated on a unit substrate to form the reconfigurable dual band bidirectional amplifier shown in Fig. 15. As can be seen in Fig. 15, there are transition lines between each reflection amplifier and the BLC's ports. These transition lines tune the input impedance of the reflection amplifiers in order to minimize the VSWR in the in/output port of the bidirectional amplifier and help compensate any mismatch in frequency response in the reflection amplifiers. Figure 16 shows the results of measurement and simulation for the reconfigurable dual band bidirectional amplifier. The tuning capacitor value C_t location is optimized with ADS and then tuned during the measurements. The minimum gain is 11.2 dB at the 2.4 GHz frequency band.

B. Reconfigurable Dual Band Active Van Atta Array

The Van Atta array is an arrangement to form an RDA system and it has found many applications in wireless communication due to its simple configuration [5], [18], [35] and [36]. As shown in Fig. 17, in the Van Atta array configuration each pair of antenna elements are located symmetrically with respect to the center of the array and are connected together by a transmission line. These transmission lines may have different physical length, but their electrical length should have a $2n\pi$ phase shift with respect to each other [18]. Thus, the signal received by each element from a plane wave incident with angle θ as indicated in Fig. 17 appears at its pair through the inter connecting transmission line. Each element receives and re-radiates electromagnetics field simultaneously. The phase distribution of the reradiated field is reversed with respect to the received field, which leads to having the same reradiating angle as the received field, Fig. 17. The scattered field radiation pattern is related to the number of Van Atta array elements and their radiation pattern according to [37]

$$E_{total}^{passive}(\theta) \propto M_p U^2(\theta), \tag{6}$$

where M_p is the number of antenna elements in the passive Van Atta array and $U(\theta)$ is the radiation pattern of each antenna element. Therefore, Eq. ((6)) implies that a larger number of array elements is needed to increase the strength of the scattered field, but this solution would complicate the layout of the feed network.

The Active Van Atta array is the solution to increase the scattered field power by using unilateral or bilateral amplifiers in the inter-connecting transmission lines [13], [38]. The unilateral amplifiers allow only half of the elements to receive the signal and the other half to reradiate it. On the other hand, with bidirectional amplifiers all the elements receive and reradiate the signal simultaneously, yielding

$$E_{total}^{active}(\theta) \propto M_a G U^2(\theta), \tag{7}$$

where M_a is the number of antenna elements in the active Van Atta array and G is the gain of each bidirectional amplifier.

In this work, a novel reconfigurable dual band active Van Atta array using two dual band antenna elements integrated with our bidirectional amplifier is presented. To the

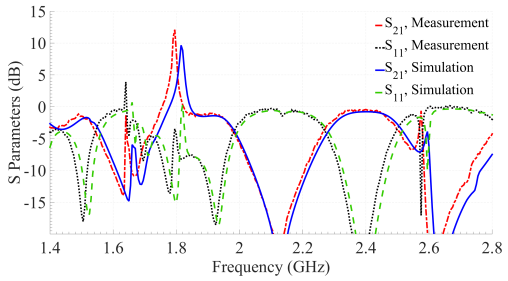

(a)

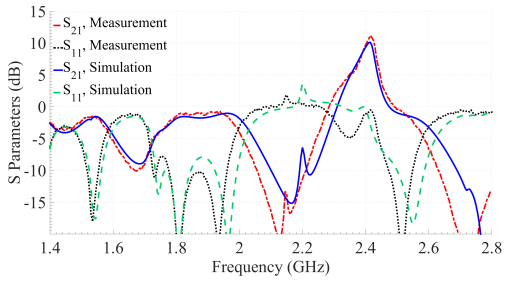

(b)

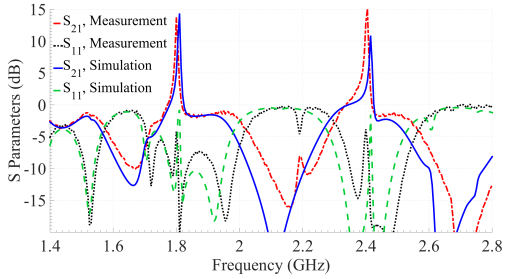

(c)

Fig. 16: The measurements and simulations of the reconfigurable dual band bidirectional amplifier. (a) 1.8 GHz frequency band, $V_{D1} = 5$ V and $VD2 = 5$ V, (b) 2.4 GHz frequency band, $V_{D1} = 0$ V and $V_{D2} = 5$ V and (c) 1.8 GHz and 2.4 GHz frequency bands, $V_{D1} = 5$ V and $V_{D2} = 0$ V. Measurements are black lines and simulations are gray lines.

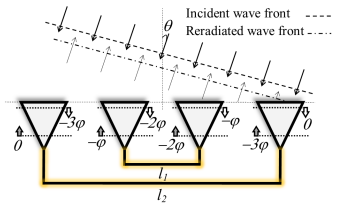

Fig. 17: The Van Atta array configuration.

best of the authors' knowledge, an active Van Atta array with bidirectional elements has been presented only for the case of single band in [13]. In addition, a passive Van Atta array has been presented for dual band operation in [39], however its feed network becomes complex using synthesized microstrip lines to separate the signal paths in each frequency bands and to maintain the required phase condition. The results show that our system with two elements re-scatters the incoming field with higher strength compared to a four-element passive

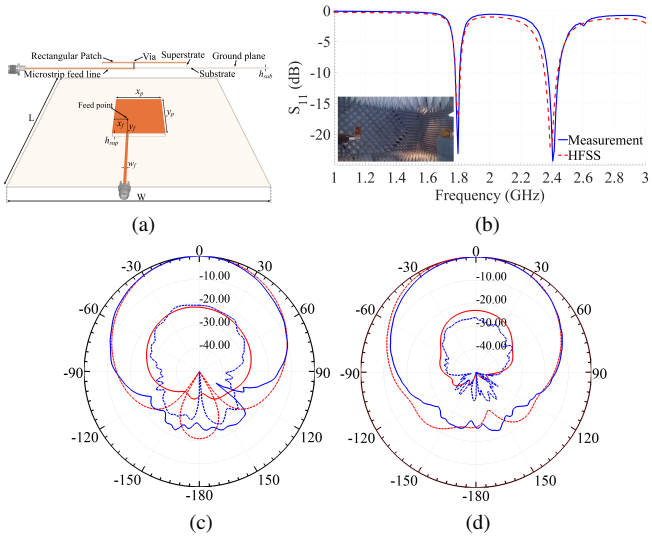

(a) (b)

(c) (d)

Fig. 18: (a) The dual band rectangular microstrip patch antenna, (b) the antenna S_{11}, (c) normalized radiation pattern at 1.8 GHz and (d) at 2.4 GHz. The solid lines are co-pole radiation and dashed lines are cross-pole radiation patterns.

Van Atta array with the same dual band antenna elements in each frequency band.

Any dual band antenna can be used to form the dual band active Van Atta array. Here, a pin fed rectangular microstrip patch antenna is used as the antenna element, Fig. 18(a). The substrate is Rogers 4003C with $h = 0.812$ mm (32 mil) and the superstrate is RT duroid 5880 with $\epsilon_r = 2.2$ and $h = 3.175$ mm (125 mil). The antenna resonant frequencies are determined by the dimension of the patch [40]. The radiation edge in the lower (higher) frequency band is the longer (shorter) edges of the patch. The antenna operates in the 1.8 GHz and 2.4 GHz frequency bands with vertical and horizontal polarization, respectively. The antenna S_{11} is shown in Fig. 18(b) and the radiation pattern in co- and cross-polarization are shown in Fig. 18(c) and 18(d), respectively. The antenna gains are 7.5 dBi and the -3 dB Half Power Beam Widths (HPBW) are $80°$ and $90°$ at 1.8 GHz and 2.4 GHz, respectively.

For simplicity, the fabricated bidirectional amplifier and the antenna elements were connected with SMA connectors, as shown in Fig. 19(a); however one could fabricate everything on the same planar circuit.

To investigate the benefit of our design with the passive Van Atta array, a comparison has been done between the two-element active Van Atta array of Fig. 19(a) and the four-element passive Van Atta array of Fig. 19(b). The distance between the array elements is $0.35\lambda_0$ and $0.5\lambda_0$ at 1.8 GHz and 2.4 GHz, respectively.

As can be seen in Fig. 19(a), the plane wave with vertical (horizontal) polarization at 1.8 GHz, $\mathbf{E}_{1.8\text{ GHz}}$ (2.4 GHz, $\mathbf{E}_{2.4\text{ GHz}}$) is incident on the proposed active Van Atta array with the angle is θ_0. The signal received by each of the patch antennas is amplified by the bidirectional amplifier with the gain of G and then re-radiated by the other antenna. The re-

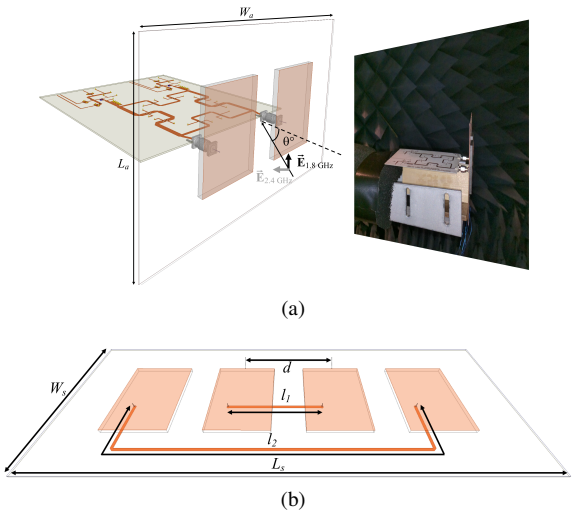

Fig. 19: (a) The active reconfigurable dual band Van Atta array and (b) the passive Van Atta with four antenna elements. All dimensions in mm are: $L_s = 300$, $W_s = 110$, $L_a = 110$, $W_a = 160$ $d = l_1 = 62.5$, $l_2 = 261$ for operating at 1.8 GHz and $l_2 = 286$ for operating at 2.4 GHz.

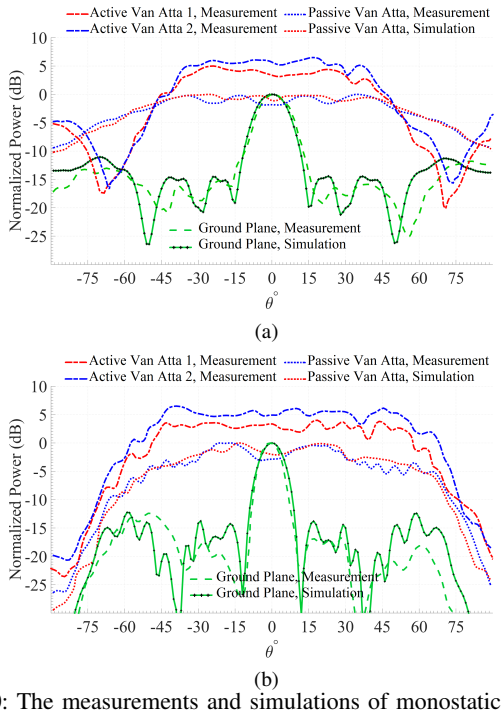

Fig. 20: The measurements and simulations of monostatic RCS as a normalized power at (a) 1.8 GHz frequency band, and (b) 2.4 GHz frequency band.

radiated field toward the interrogator is G times higher than the received field.

Results of RCS measurements and simulations for the active Van Atta array with two antenna elements, the passive Van Atta array with four antenna elements, and a ground plane with size $L_s \times W_s$ as a non-retrodirective scatterer element for comparison, are shown in Fig. 20. Recalling that the active Van Atta array contains dual band reflection amplifiers that can operate either in single band mode or in dual band mode, we examine the RCS for both modes and refer to the single band mode as active Van Atta 1 and to the dual band mode as active Van Atta 2.

In Fig. 20(a), we examine the monostatic RCS at 1.8 GHz and obtain that an average 4.5 dB and 6 dB higher gains have been accomplished by the two-element active Van Atta 1 and 2, respectively, compared to the four-element passive Van Atta array.

In [13], it is shown, by comparing Eq. (6) and Eq. (7), that $G = \zeta_{dB} + 6$ dB, where ζ is the ratio of the back-scattered field levels of the passive and active array when $M_p = 2 \times M_a$. Thus, the gains of the bidirectional amplifier when it is connected to the antennas are 10.5 dB and 12 dB for cases 1 and 2, respectively. The measured gain from Fig. 16(a) and Fig. 16(c) is 10 dB and 13.7 dB, respectively.

It should be noticed that the bidirectional amplifier gain is measured by a network analyzer. However, the input impedance of the antennas are not perfectly 50 Ω and this may slightly influence the bidirectional amplifier gain. The -3 dB HPBW of the monostatic RCS of the active array is about 90° and it shows the range of angle values for which there is satisfactory self-steering capability of the Van Atta array. In addition, there is a discrepancy between the active and passive array monostatic RCS, which is more noticeable at 1.8 GHz. There are three possible causes that could contribute to the discrepancy between the active and passive monostatic patterns. One possible cause is the electrical size of the array aperture, which is larger for the passive array. Another possible cause is the electrical distance between consecutive array elements and the associated mutual coupling. A third possible cause is the interconnection between the antennas and the circuit, which has been discussed in [13].

Figure 20(b) shows the monostatic RCS results at 2.4 GHz. The two-element active Van Atta 1 and 2 shows 3.75 dB and 5.75 dB higher gain on average compared to the four-element passive Van Atta array, see Fig. 20b. Thus, the gain of the bidirectional amplifier, when it is connected to the antennas, is 9.7 dB and 11.75 dB, for case 1 and 2, respectively. The measured gain from Fig. 16(b) and Fig. 16(c) is 10 dB and 13 dB, respectively. The -3 dB HPBW of the active array is around 100°.

IV. Conclusion

We proposed a novel reflection amplifier which is able to reconfigure its operation frequency band in two different bands independently. The reflection amplifier is realized using a HJ-FET transistor, and two PIN diodes to form a reconfigurable load. This configurability is achieved by two control voltages with low (high) level, 0 V (5 V). This reflection amplifier is capable to be also used in RFIDs or active scatterer applications. Using two frequency bands allow an agile system to change the operation frequency band, something needed in crowded spectrum or smart communication systems. It also increases the channel capacity if both frequency bands are used, since the dual operation frequency band can be achieved independently.

The proposed reflection amplifier is integrated with a dual band BLC to make a reconfigurable dual band bidirectional

amplifier. This bidirectional amplifier is used to feed two dual band patch antennas to form an active Van Atta array. The proposed active array operates in two frequency bands and offers four operating modes: i) 1.8 GHz only, ii) 2.4 GHz only, iii) dual band 1.8 GHz and 2.4 GHz and iv) being off. The proposed active Van Atta array outperforms passive antenna arrays using half of the number elements.

V. Acknowledgment

This work was partially funded by the US National Science Foundation CAREER award 1620902. The authors are thankful to the Reviewers for their constructive comments.

References

[1] H. Stockman, "Communication by means of reflected power," *Proceedings of the IRE*, vol. 36, no. 10, pp. 1196–1204, Oct 1948.

[2] K. Finkenzeller, *RFID Handbook: Fundamentals and Applications in Contactless Smart Cards, Radio Frequency Identification and near-Field Communication, Third Edition*. New York, NY, 10158: John Wiley & Sons,Inc., 2010.

[3] E. Kampianakis, J. Kimionis, K. Tountas, C. Konstantopoulos, E. Koutroulis, and A. Bletsas, "Wireless environmental sensor networking with analog scatter radio and timer principles," *IEEE Sens. J.*, vol. 14, no. 10, pp. 3365–3376, Oct 2014.

[4] B. S. Hewitt, "The evolution of radar technology into commercial systems," in *Microwave Symposium Digest, 1994., IEEE MTT-S International*, May 1994, pp. 1271–1274 vol.2.

[5] E. Gruenberg and C. Johnson, "Satellite communications relay system using a retrodirective space antenna," *IEEE Trans. Antennas Propag.*, vol. 12, no. 2, pp. 215–223, Mar 1964.

[6] B. Smida and S. Islam, "Full-duplex wireless communication based on backscatter amplifier," in *2014 IEEE International Conference on Communications Workshops (ICC)*, June 2014, pp. 91–95.

[7] E. Mattei, E. Lucano, F. Censi, M. Triventi, and G. Calcagnini, "Provocative Testing for the Assessment of the Electromagnetic Interference of RFID and NFC Readers on Implantable Pacemaker," *IEEE Trans. Electromagn. Compat.*, vol. 58, no. 1, pp. 314–322, Feb 2016.

[8] J. Kimionis, A. Georgiadis, A. Collado, and M. M. Tentzeris, "Enhancement of RF Tag Backscatter Efficiency With Low-Power Reflection Amplifiers," *IEEE Trans. Microw. Theory Tech.*, vol. 62, no. 12, pp. 3562–3571, Dec 2014.

[9] P. Chan and V. Fusco, "Bi-static 5.8 GHz RFID range enhancement using retrodirective techniques," in *Microwave Conference (EuMC), 2011 41st European*, Oct 2011, pp. 976–979.

[10] A. Strobel, C. Carlowitz, R. Wolf, F. Ellinger, and M. Vossiek, "A Millimeter-Wave Low-Power Active Backscatter Tag for FMCW Radar Systems," *IEEE Trans. Microw. Theory Tech.*, vol. 61, no. 5, pp. 1964–1972, May 2013.

[11] J. F. Bousquet, S. Magierowski, and G. G. Messier, "A 4-GHz Active Scatterer in 130-nm CMOS for Phase Sweep Amplify-and-Forward," *IEEE Trans. Circuits Syst. I-Regul. Pap.*, vol. 59, no. 3, pp. 529–540, March 2012.

[12] C. Belfi, C. Rothenberg, L. Schwartzman, R. Tilley, and A. Wills, "A satellite data transmission antenna," *IEEE Trans. Antennas Propag.*, vol. 12, no. 2, pp. 200–206, Mar 1964.

[13] S.-J. Chung, S.-M. Chen, and Y.-C. Lee, "A novel bi-directional amplifier with applications in active Van Atta retrodirective arrays," *IEEE Trans. Microw. Theory Tech.*, vol. 51, no. 2, pp. 542–547, Feb 2003.

[14] H. I. Cantu and V. F. Fusco, "A 21 GHz Reflection Amplifier MMIC for Retro-Directive Antenna and RFID Applications," in *MM-Wave Products and Technologies, 2006. The Institution of Engineering and Technology Seminar on*, Nov 2006, pp. 66–70.

[15] G. T. Munsterman, "Tunnel-diode, microwave amplifiers," *APL Technical Digest*, May-June 1965.

[16] J. E. Carroll, "Mechanisms in Gunn effect microwave oscillators," *Radio and Electronic Engineer*, vol. 34, no. 1, pp. 17–30, July 1967.

[17] J. G. de Koning, R. E. Goldwasser, R. J. Hamilton, and F. E. Rosztoczy, "Wideband GaAs Gunn reflection amplification for the 18-26.5 GHz waveguide band," *Electron. Lett.*, vol. 11, no. 9, pp. 195–196, May 1975.

[18] L.C. Van Atta, "Electromagnetic reflector," Oct. 6 1959, US Patent 2,908,002.

[19] J. A. Vitaz, A. M. Buerkle, and K. Sarabandi, "Tracking of Metallic Objects Using a Retro-Reflective Array at 26 GHz," *IEEE Transactions on Antennas and Propagation*, vol. 58, no. 11, pp. 3539–3544, Nov 2010.

[20] T.-J. Hong and S.-J. Chung, "24 GHz active retrodirective antenna array," *Electron. Lett.*, vol. 35, no. 21, pp. 1785–1786, Oct 1999.

[21] L. Chiu, Q. Xue, and C. H. Chan, "A wideband circularly-polarized active Van Atta retrodirective transponder with information carrying ability," in *2006 Asia-Pacific Microwave Conference*, Dec 2006, pp. 231–234.

[22] D. E. N. Davies, "Some properties of Van Atta arrays and the use of 2-way amplification in the delay paths," *Electrical Engineers, Proceedings of the Institution of*, vol. 110, no. 3, pp. 507–512, March 1963.

[23] L. W. Mayer and A. L. Scholtz, "A Dual-Band HF / UHF Antenna for RFID Tags," in *Vehicular Technology Conference, 2008. VTC 2008-Fall. IEEE 68th*, Sept 2008, pp. 1–5.

[24] G. Lasser, R. Langwieser, F. Xaver, and C. F. Mecklenbräuker, "Dual-band channel gain statistics for dual-antenna tyre pressure monitoring RFID tags," in *2011 IEEE International Conference on RFID*, April 2011, pp. 57–61.

[25] J. W. Bandler, "Stability and gain prediction of microwave tunnel-diode reflection amplifiers," *IEEE Trans. Microw. Theory Tech.*, vol. 13, no. 6, pp. 814–819, Nov 1965.

[26] K. Kurokawa, "Injection locking of microwave solid-state oscillators," *Proc. IEEE*, vol. 61, no. 10, pp. 1386–1410, Oct 1973.

[27] H. I. Cantu and V. F. Fusco, "A 21 GHZ Reflection Amplifier MMIC for Retro-Directive Antenna and RFID Applications," in *mm-Wave Products and Technologies, 2006. The Institution of Engineering and Technology Seminar on*, Nov 2006, pp. 66–70.

[28] R. E. Collin, *Foundations for Microwave Engineering, 2nd Edition*. Wiley-IEEE Press, 2001.

[29] I.-H. Lin, M. DeVincentis, C. Caloz, and T. Itoh, "Arbitrary dual-band components using composite right/left-handed transmission lines," *IEEE Trans. Microw. Theory Tech.*, vol. 52, no. 4, pp. 1142–1149, April 2004.

[30] C. Caloz and T. Itoh, "Application of the transmission line theory of left-handed (LH) materials to the realization of a microstrip LH line," in *Antennas and Propagation Society International Symposium, 2002. IEEE*, vol. 2, 2002, pp. 412–415 vol.2.

[31] A. Lazaro, A. Ramos, R. Villarino, and D. Girbau, "Time-Domain UWB RFID Tag Based on Reflection Amplifier," *IEEE Antennas Wirel. Propag. Lett.*, vol. 12, pp. 520–523, 2013.

[32] P. Chan and V. Fusco, "Full duplex reflection amplifier tag," *IET Microw. Antennas Propag.*, vol. 7, no. 6, pp. 415–420, April 2013.

[33] A. S. A. Bechteler and T. F. Bechteler, "Switchless bidirectional amplifier for wireless communication systems," *Microw. Opt. Technol. Lett.*, vol. 49, no. 8, pp. 1888–1890, 2007.

[34] D. Rubin, "Millimeter-wave hybrid coupled reflection amplifiers and multiplexer," *IEEE Trans. Microw. Theory Tech.*, vol. 30, no. 12, pp. 2156–2162, Dec 1982.

[35] S.-J. Chung, T.-C. Chou, and Y.-N. Chin, "A novel card-type transponder designed using retrodirective antenna array," in *Microwave Symposium Digest, 2001 IEEE MTT-S International*, vol. 2, May 2001, pp. 1123–1126 vol.2.

[36] E. Sharp and M. Diab, "Van Atta reflector array," *IRE Transactions on Antennas and Propagation*, vol. 8, no. 4, pp. 436–438, July 1960.

[37] S.-J. Chung and K. Chang, "A retrodirective microstrip antenna array," *IEEE Trans. Antennas Propag.*, vol. 46, no. 12, pp. 1802–1809, Dec 1998.

[38] H.-T. Chen and S.-J. Chung, "Design of a planar array transponder with broad responding beam," *IEEE Microw. Guided Wave Lett.*, vol. 7, no. 9, pp. 297–299, Sep 1997.

[39] J. W. Tsai, C. H. Wu, and T. G. Ma, "Novel dual-mode retrodirective array using synthesized microstrip lines," *IEEE Trans. Microw. Theory Tech.*, vol. 59, no. 12, pp. 3375–3388, Dec 2011.

[40] C. A. Balanis, *Antenna theory: analysis and design*. John Wiley & Sons, 2016, 4th edition.

Farhad Farzami (S'10) received his B.S. degree in electrical engineering from University of Tabriz in 2009 and M.S degree in microwave engineering from Tarbiat Modares University in 2012, Tehran, Iran. He is currently a Ph.D. student in the Andrew Electromagnetics Laboratory at the University of Illinois at Chicago (UIC). His research interests include active and passive front-end microwave circuits and antenna design; metamaterial based RF circuits for investigating wave propagation in uniaxial media and antenna miniaturization by using ultra-thin magneto-dielectric substrates; backscattering communication for full duplex and RFID applications, design, simulation and fabrication of analog self-interference cancellation circuits and antenna systems; reconfigurable antennas and front-end microwave circuits for Software Defined Radio applications. In addition, he is a member of the Networks Information Communications and Engineering Systems Laboratory (NICEST) at UIC to realize In-Band Full-Duplex Communications for 5G systems.

Seiran Khaledian (S'11) received her B.S. degree in electrical engineering from Khaje Nasir University of Technology (KNTU) in 2010 and M.S degree in microwave engineering from Tarbiat Modares University in 2013, Tehran, Iran. She is currently a Ph.D. student at the University of Illinois at Chicago (UIC). Her research interests are in realization of 5G wireless communication systems, including full-duplex communication systems, analog self-interference cancellation techniques and reconfigurable antenna and RF/microwave components.

Besma Smida is an Associate Professor of Electrical and Computer Engineering at University of Illinois at Chicago. After completing her appointment as a Postdoc and later a Lecturer at Harvard University, she became an Assistant Professor of Electrical and Computer Engineering at Purdue University Calumet. Additionally, she was a Research Engineer in the Technology Evolution and Standards group of Microcell, Inc. (now Rogers Wireless), Montreal, Canada. Dr. Smida took part in wireless normalization committees (3GPP, T1P1). She obtained the Ph. D. and M. Sc. from the University of Quebec (INRS), Montreal, Canada. Her research focuses on wireless communication theory. She received the Academic Gold Medal of the Governor General of Canada in 2007 and the NSF CAREER award in 2015.

Danilo Erricolo (S'97-M'99-SM'03-F'16) received the Laurea degree of Doctor (summa cum laude) in electronics engineering from the Politecnico di Milano, Milan, Italy, in 1993 and the Ph.D. degree in electrical engineering and computer science from the University of Illinois at Chicago (UIC), Chicago, Illinois, USA, in 1998. He is a Professor in the Department of Electrical and Computer Engineering, UIC, where he is also the Director of the Andrew Electromagnetics Laboratory, and an adjunct Professor of Bioengineering. During summer 2009, he was an Air Force Faculty Fellow at the Air Force Research Laboratory, Wright-Patterson Air Force Base, Dayton, Ohio, USA. He has authored or coauthored more than 240 publications in refereed journals and international conferences. He has served as Associate Editor of the IEEE Antennas and Wireless Propagation Letters (2002-2014), the IEEE Transactions on Antennas and Propagation (2013–2016) and Radio Science (2014-2016). In 2006, he was the Guest Editor of the Special Issues on RF Effects on Digital Systems of the Electromagnetics Journal, and in 2012 he was the Lead Guest Editor of the Special Issue on Propagation Models and Inversion Approaches for Subsurface and Through Wall Imaging, of the International Journal of Antennas and Propagation. His research interests are primarily in the areas of electromagnetic propagation and scattering, high-frequency techniques, wireless communications, electromagnetic compatibility, the computation of special functions, and magnetic resonance imaging. He developed a 2D simulator for the propagation of the electromagnetic field in urban environments that could consider base-stations located below or above the average rooftop height, thanks to introduction of uniform theory of diffraction double wedge diffraction coefficients. He contributed to the development of many exact solutions of canonical scattering problems, which advance the understanding of scattering from analytically treatable geometries and provide benchmarks for computational electromagnetics software. As part of these studies, he wrote software for the computation of Mathieu functions that has applications beyond the field of electrical engineering. He also developed an acceleration method for series expansions containing Mathieu, prolate and oblate spheroidal functions, which impacts all applications of these functions, such as in porous media flow. He contributed to the validation of the incremental theory of diffraction by developing comparisons with exact canonical solutions and experiments. He co-authored the first papers on RF tomography for applications to subsurface sensing and is currently engaged with its extension to other environments. He also applied his research to medical applications, specifically in the field of magnetic resonance imaging. Dr. Erricolo is a Fellow of IEEE, a member of Eta Kappa Nu and was elected a Full Member of the U.S. National Committee (USNC) of the International Union of Radio Science (URSI) Commissions B, C, and E. He served as Chair (2009- 2011), Vice Chair (2006-2008) and Secretary (2004-2005) of the USNC-URSI Commission E on Electromagnetic Environment and Interference. Between 2009 and 2014, he served as Chair of the USNC-URSI Ernest K. Smith Student Paper Competition. He also served as Vice-Chair of the Local Organizing Committee of the XXIX URSI General Assembly, held in Chicago, Illinois, USA in August 2008. He serves as Member at Large of USNC-URSI (2012-2017), a committee of the US National Academies. He was the General Chairman of the 2012 IEEE International Symposium on Antennas and Propagation and USNCURSI National Radio Science Meeting, held in Chicago, Illinois, USA in July 2012. Between 2011 and 2016, was Chair of the Chicago Joint Chapter of the IEEE Antennas and Propagation Society (AP-S) and Microwave Theory and Techniques Society (MTT). Since 2005, he has served on the IEEE AP-S Future Symposia Committee and, since 2006, he has served (as a USNC-URSI representative) on the AP-S/USNC-URSI Joint Meetings Committee. He was an Elected Member of the Administrative Committee of the IEEE AP-S (2012-2014) and served as Chair of the Distinguished Lecturer Program of the IEEE AP-S (2015-2016). He has served on more than 40 conference technical program committees, chaired over 60 conference sessions, and organized more than 20 special sessions at international scientific conferences.